

# Matrix Adaptive SHrinkage: A model for Estimating Effects Across Tissues applied to the GTEx dataset

Sarah Urbut <sup>1,2</sup>, Gao Wang <sup>1</sup>, Matthew Stephens <sup>1,3,†</sup>, with the GTEx Consortium<sup>¶</sup>

**1** Department of Human Genetics/ University of Chicago, Chicago, IL USA

**2** Pritzker School of Medicine/Growth and Development Training

Program/University of Chicago, Chicago, IL USA

**3** Department of Statistics/ University of Chicago, Chicago, IL USA

## Abstract

## Author Summary

Variation in gene expression is an important mechanism underlying susceptibility to complex disease. The simultaneous genome-wide assay of gene expression and genetic variation allows the mapping of the genetic factors that underpin individual differences in quantitative levels of expression (expression QTLs; eQTLs). By analyzing these effects across multiple tissues, we exploit the information that the effect of the gene-snp pair in one tissue can provide about its effect in alternative tissues. Furthermore, quantifying the effect size as opposed to simply calling QTLs present or absent reveal many patterns of sharing of effects among tissues which differ in both sign and magnitude. We provide a novel framework for estimating effect sizes across multiple subgroups, considering the evidence contained in all subgroups jointly, which provides a powerful and detailed insight into quantitative heterogeneity present in the genome.

## Introduction

Variation in gene expression is an important mechanism underlying susceptibility to complex disease. The simultaneous genome-wide assay of gene expression and genetic variation allows the mapping of the genetic factors that underpin individual differences in quantitative levels of expression (expression QTLs; eQTLs). The availability of this information provides immediate insight into a biological basis for disease associations identified through genome-wide association (GWA) studies, and can help to identify networks of genes involved in disease pathogenesis ([1,2]). Available methods are limited not only in their ability to *jointly analyze data on all tissues* to maximize power, but also in simultaneously *allowing for both qualitative and quantitative differences among eQTLs* present in each tissue.

Initial approaches to quantify the effect of a particular SNP on gene expression considered only one tissue at a time, and ignored the effect of the SNP on gene expression in other tissues. This failed to exploit the power of shared genetic variation in effects on expression - i.e. the information that the effect of the gene-snp pair in one tissue can provide about the effect in another- and limited our understanding of multiple-tissue phenotypes. Furthermore, even past attempts at quantifying heterogeneity of eQTLs using the data across tissues jointly were limited in both the number of tissues considered, and also the level of heterogeneity considered. Qualitative heterogeneity refers to calling a snp ‘active’ or ‘inactive’ in a given tissue. For example, previous attempts at joint analyses referred to the setting in which the gene-snp pair is active in all tissues as ‘shared’ and active in only one as ‘tissue-specific’ ([3,4]). However, a QTL may be ‘active’ in all or many tissues and with varying magnitude or sign; we refer to this as quantitative heterogeneity.

Indeed, our initial motivation came from our group’s past analysis of GTEx pilot data [?], in which we saw evidence that many (50%) QTLs are shared across all nine tissues. In this context, a QTL was called based on whether it demonstrates significant posterior probability of being active in a particular tissue. Applying our previous hierarchical model (‘eQTL-BMA’) to the dataset from Dimas *et al* [5] with 3 tissues, we found just 8% of eQTLs were specific to a single tissue, with an estimated 88% of eQTLs being common to fibroblasts, LCL cells and T-Cells [3]. Not all eQTLs are shared by all tissues; some tissues may share eQTLs more than others. To allow for this, our previous hierarchical model attempted to infer the extent of such sharing by estimating the proportion of eQTLs which were shared in various ‘configurations’ or patterns of binary activity in which a QTL was ‘called’ or ‘absent’ in each tissue. However, these binary configurations were still *limited in their ability to capture continuous variation* in levels of activity among tissues in which the SNP is considered active. In fact, as the number of tissues considered increases, perhaps the more interesting and biologically relevant question becomes one of quantitative heterogeneity - that is, how do the patterns of effect vary across tissues in which the SNP is called ‘active’.

The novel approach we offer here allows groups of QTLs to be classified not only by their presence or absence in a particular tissue, but by their *relationships in continuous effects between tissues*, e.g., consistently larger effects in some tissues than other. Critically, quantifying the effect sizes of the gene-snp pair across tissues considering the evidence contained in all tissues jointly thus reveals new patterns of activity across tissues, which differ in their relationship in sign and magnitude within and between tissues. The novel framework described here allows that these effects be ‘shared’ but not necessarily ‘consistent’ across tissues, thus capturing continuous variation heretofore missed. The structure of this paper is as follows: we will describe our approach in brief for modeling and estimating these effect sizes across tissues, demonstrate the utility of such an approach on simulated data, and apply our method to data from the GTEx dataset, version 6.0, where we analyze effects size for 16,069 genes across 44 tissues. In

so doing, we offer novel insight into the patterns of quantitative heterogeneity in genetic effects among a greater number of tissues than ever analyzed before.

53

54

## 0.1 Methods Overview: Approach

We assume we have noisy observations of many ‘effects’ in many conditions. Our goals include estimating the sizes of the actual effects, including some measure of ‘significance’. In doing this we aim to exploit the fact that effects in different conditions may often be similar though not identical, while leaving open the potential to identify effects that are ‘specific’ to only some of the conditions. Critically, we allow for subtle differences among those effects that are ‘similar’. Here, we aim to learn about patterns of sharing of effects across tissues. Because these patterns are shared among SNPs, we can use the information contained in the larger data-set to help us better understand the global and SNP-specific patterns of effects of genetics on gene expression. This allows us to make comparisons among tissues in which the QTL is called active, and among gene-SNP pairs with a similar degree of activity in a given tissue.

Here, we assume that each eQTL may follow a particular pattern of activity characterized by its effects across tissues. Within these groups, the tissues exhibit characteristic patterns of sharing, which can be captured by considering the covariance structure of the genetic effects among tissues. This lends itself to a mixture model, in which we assume all the gene-SNP pairs arise from a mixture of a finite number of multivariate normal (MVN) distribution, each characterized by the covariance matrix from which the vector of effects is thought to arise. For each of  $J$  gene-SNP pairs, we observe an  $R$  dimensional vector of standardized effect sizes and their standard error and assume that these effects descend from some true effect size  $\mathbf{b}$ .

$$\mathbf{b}_j | \boldsymbol{\pi}, \mathbf{U} \sim \sum_{k,l} \pi_{k,l} N_{\mathbf{R}}(\cdot; \mathbf{0}, \omega_l \mathbf{U}_k) \quad (1)$$

To capture both similarity and differences of effects across tissues we assume that each effect arises from one of  $K$  ‘classes’. For example, one class could represent effects that are shared (‘shared class’);

and another class could represent effects that are specific to the first condition, or some other subset of conditions (i.e. are zero or close to zero in other conditions). For each class we allow that effects may come from one of  $L$  ‘sizes’. For example, among effects that are of a ‘shared’ class, some may be ‘shared’ by all tissues and consistently large and others may be ‘shared’ by all tissues but consistently moderate. Critically, although we use phrases such as ‘consistent’ and ‘large’ here for convenience, our model allows for a range of actual quantitative values within each class-size combination (see 1 ). Thus, in the ‘shared’ class, effects may be active under all conditions, but with varying degrees of activity in each tissue; or active with quantitative variation in a subset of conditions, and small but non-zero in other conditions. Specifically we assume that the effects  $\mathbf{b}$  come from a mixture model (Equation 1) here, where the matrix  $U_k$  determines the similarity of effects among conditions for class  $k$ , and the scalar  $\omega_l$  determines the typical size of effect for size  $l$ . The parameters  $\pi_{k,l}$  capture the relative frequency of each class-size combination, and estimating these parameters from the data is one key step in fitting this model.

Thus the covariance matrix  $U_k$  captures the particular patterns of sharing reflecting the variation in effect sizes within and between tissues, while  $\omega_l$  determines the scale of each pattern - the magnitude of the effect size. The relationship among the distinct entries of this matrix allows us to specify effects which may be consistently larger in some tissues relative to others and may possess variable correlation among different pairs of tissues (e.g., see Figure 1, **B**, for converse relationships among effects in tissue one and two for SNPs of green opposed to blue class). Thus we also recognize that while two eQTL may obey a similar pattern or shape, the absolute scale may vary. For example, two eQTL may both have strong correlation between liver and lung with consistently larger effects in liver, but the absolute size of the effects may vary between

104  
105

SNPs (Figure 1, **A**, contrast gene-snp pairs of far left and far right pattern). Critically, these patterns are learned from the data rather than forced.

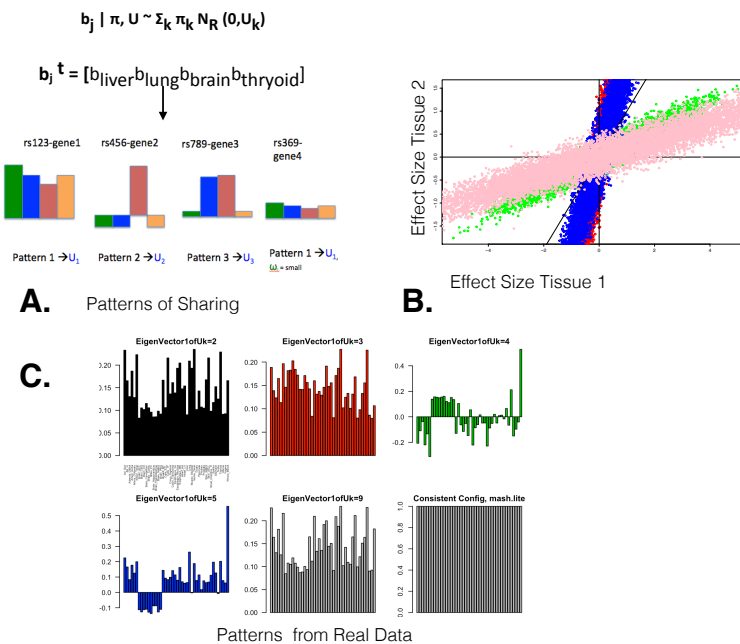


**Figure 1. Modeling Many Patterns of Sharing.** **A:** Here, we display a variety of patterns of sharing present in the data. eQTLs belonging to the first class have large positively correlated effects that are consistent in sign though heterogeneous in magnitude. eQTL of pattern 2 display weak consistent effects in liver, lung and thyroid that are inversely correlated with strong tissue specific effects in brain, while eQTL of pattern 3 demonstrate strong effects in a select group of tissues (here, lung and brain), but quantitatively weaker though correlated in sign with liver and thyroid. eQTL of the fourth group show patterns similar in ‘shape’ to eQTL in class 1, though their absolute scale is smaller. **B:** In this two tissue-example, a model which simply calls QTLs ‘active’ or ‘inactive’ assumes that all effects fall along the x, y or 45 degree (1,1) line: estimating heterogeneous effects which may be consistently larger in some tissues relative to others and may possess variable correlation among different pairs of tissues allows us to capture more diverse biological patterns. **C:** In these examples from real data, we illustrate patterns that were ‘learned’ from the data and demonstrate a varying range of quantitative values among tissue we’ve deemed active. Note  $U_k$  2,3 and 9 demonstrate consistent though quantitatively heterogeneous effects, while patterns 4 and 5 show varying levels of tissue specificity. Contrast that with the mash-lite approach to consistency, which only allows for homogenous effects throughout.

## 0.2 Previous Approach

106  
107  
108  
109  
110  
111  
112  
113

Previous work from our lab considered the idea of configuration - i.e., that a gene-snp pair was simply ‘active’ or ‘inactive’ in a particular tissues - and thus for R tissues, there were  $2^R$  possible configurations, which becomes computationally infeasible as  $R$  grows. Thus a non-trivial novelty of our approach is its application to joint estimation of effects across a larger number of  $R= 44$  tissues, never before described.

Furthermore, this considered only the idea that the variance in effect sizes between two tissues was the same across tissues thought to be active and the covariances were

also the same among tissues thought to be active in a given ‘configuration’, and thus failed to incorporate the much richer covariance structure between tissues. For example, many gene-SNP pairs might follow a pattern in which it is common to be ‘active’ across all tissues, but some QTL may have consistently larger effects in liver, lung and thyroid while other QTL may possess consistently larger effects in brain tissues and still another class of gene-snp pairs may show consistently quantitatively specific activity in whole blood but non-trivial effects in other tissues.

As a critical innovation on our previous work [3,4] the covariance matrices used here contain distinct diagonal and off-diagonal elements which reflect data-specific patterns of variation within and covariance between subgroups (tissues). This captures the variation in effect sizes within and between subgroups better than restricting effects to simply ‘shared’ or ‘unshared’. This effectively amounts to a random effects analysis in which we assume that the between subgroup variability, here the entries of the matrix  $U_k$  is unique for each study (see Borenstein et al).

Because we can’t know the ‘true covariance matrix’ for each gene-snp pair, we aim to assemble a list which sufficiently captures the various patterns, and then ‘learn’ the relative proportions of each pattern of sharing from the data. One can now model each vector of effect sizes  $b_j$  as arising from a mixture that captures all the covariance patterns present (Equation 1).

The primary novelty of this approach is *to estimate this multivariate posterior distribution on the effect size in a data-sensitive way* - i.e., using the mixture model to capture information about the covariance structure among subgroups (here, tissues), and thus describe the heterogeneity of effects across tissues, rather than simply calling effects ‘shared’ or ‘specific’. We deem this model ‘hierarchical’ because these prevailing patterns of activity are learned from the larger dataset - e.g., a large, random set of gene-snp pairs - and influence our inference about a given gene-snp pair ‘j’. Thus we might identify a situation in which it is common to have large effects in certain tissues and not others. Accordingly, if a given observed gene-snp pair demonstrates a small effect in one of the ‘off issues’, we might be inclined to conclude that it is indeed a member of this particular class and shrink the small effect in this tissue accordingly without reducing our estimates of the more ‘active tissues’. However, if we observe the same small effect in a setting in which ‘similar tissues’ have large effects, we might ‘shrink’ this effect size less, due to our high prior belief in the SNP’s effectiveness garnered from adjacent tissues. Thus we deem this method ‘Adaptive Shrinkage’ because the appropriate amount of shrinkage is learned from the overall dataset. Critically, our method is dually adaptive, in the sense that we learn the relative abundance of effect sizes and directions from the overarching data set: observed effects are nudged towards prevailing patterns and sizes, according to the learned proportions of each.

Because our prior belief in consistency is strong in this particular dataset, we identify many more ‘significant associations’ in settings where perhaps the observed univariate statistic in one tissue is small but otherwise large in additional tissues, nudging these effects towards something more consistent. This is in contrast to a univariate shrinkage approach, in which all effects of the same size would be ‘shrunk’ equivalently, due to lack of information garnered from adjacent tissues.

Critically, in learning about the effect size of a gene-snp pair in each tissue, we can make statements about the degree of heterogeneity present in the data-set: that is the proportion of SNPs who exhibit effects that vary in magnitude or sign. Conversely, we can describe the degree of homogeneity should these phenomena be rare. Thus we offer an additional description to eQTL analysis: the degree of heterogeneity across multiple subgroups in both sign and magnitude, by characterizing a particular QTL by the similarity in size of its effects across subgroups.

## 1 Results

### 1.1 Demonstrating Features of the Method

To get a sense of the accuracy of our novel approach to estimating multivariate effects, we simulated two types of data: shared, and tissue specific. In both settings, in which we expect our method to be superior to both univariate methods and joint methods in which the configuration approach is utilized, we simulate 50,000 gene-snp pairs, with only 400 representing true signal. This represents roughly 500 genes with 100 SNPs in cis, 80% of which contain one active QTL. Thus naturally, if the gene contains such a QTL, it is the same QTL among all tissues in which the tissue is active. This puts a dual burden on the ability of the method to accurately capture effect-sizes and shapes: the small number of true associations present in these simulations tests whether the method accurately encourages small observed effects toward zero while preserving the true signal when it exists. Furthermore, the multivariate nature of these simulated ‘true’ effects tests the ability of the method to accurately infer patterns of sharing from the dataset. These 400 true effects are thus simulated from the ‘learned’ covariance matrices representing  $U_k$  2-9 in the GTeX dataset according to (1) and thus aim to emulate the patterns of sharing present in real biological data. We then simulate vectors of observed  $\hat{\beta}_j$  and their corresponding  $Z_j$  for all 50,000 gene-snp pairs (the majority of which represent ‘noise’) according to (5) (see Methods 2.7) for details. We call this the ‘sharing’ (S) scenario.

We compare with univariate ‘shrinkage’ method Ash (Stephens *et al*, unpublished) as well as a modified version of eqtlBMA-lite (Flutre *et al*, 2013), here deemed ‘mash-lite’ which uses the singleton and fully consistent (i.e., active in only one tissue, or active with the same effect-size in all tissues) configurations to estimate these effects jointly (see Methods 2.1 item 6 for details). One might expect that our method would prove superior only in the setting in which true effects are shared among all tissues, and thus fail in the setting of tissue specificity. Thus, building on the situation above, we add a simulation in which 35% of the true effects are active in only one tissue, according to 5 different patterns of tissue specificity. We call this the ‘tissue-specific’ (TS) scenario.

We see that in terms of both power and accuracy, Matrix Ash, here deemed ‘MASH’ is superior under each simulation setting, to both univariate methods and to existing joint analysis approaches (mash-lite).

$$RMSE = \sqrt{\left( \sum_{jr} (b_{jr} - E(b_{jr}|Data))^2 \right)} \quad (2)$$

To demonstrate the ability of MASH to powerfully capture these accurately estimated effect-sizes, we compare the proportion of true associations called significant at a given significance threshold among the three methods. Indeed, MASH proves superior to both methods under each condition (i.e., sharing or tissue-specific). Once called, we can ask in how many of the cases is the sign of the estimated effect correct; again, our ability to correctly identify the direction of the effect is correct more often using our method than any other.

In introducing a method to quantify the heterogeneity of effect-sizes, we have developed a ‘heterogeneity index’ which attempts to capture the heterogeneity in magnitude among tissues in which the gene-SNP pair is active. For each gene-snp pair  $j$ , we normalize its vector of effects  $b_j$  across tissues by the effect which has the maximum absolute value; thus for a fully ‘consistent’ gene-snp pair in which all the effects are equal in magnitude, the new vector of normalized effects would consist of all ones, and R=44 tissues would be greater than 50% of the maximum effect. By contrast, for a tissue-specific gene-snp pair, the vast majority of effects would be a small fraction of the

**Table 1.** Power and Accuracy Comparison

Inference Method	MASH	ASH	mash-lite
$\text{RMSE}_S$	0.010	0.030	0.047
$\text{RMSE}_{TS}$	0.008	0.025	0.043
PTA Called NonZero at $\text{IFSR}_S 0.05$	0.758	0.20	0.52
PTA Sign Called Correctly at $\text{IFSR}_S 0.05$	0.756	0.20	0.49
PSA Incorrectly Signed at $\text{IFSR}_S 0.05$	0.0028	0.002	0.039
PTA Called NonZero at $\text{IFSR}_{TS} 0.05$	0.756	0.20	0.52
PTA Sign Called Correctly at $\text{IFSR}_{TS} 0.05$	0.754	0.20	0.49
PSA Incorrectly Signed at $\text{IFSR}_{TS} 0.05$	0.0056	0.001	0.043

**Table 2. Accuracy Analysis** Above we compare the ability of Matrix Ash ('MASH') to capture the true effect-size estimates. We compare with univariate-shrinkage method 'ASH' and configuration-specific joint approach 'mash-lite'. We report the Root Mean Squared Error (RMSE) under both settings and see a superior performance. Furthermore, in both settings we can consider the proportion of true-associations correctly called non-zero, and the proportion correctly signed, at a given significance threshold. Lastly, to calibrate our method, we can ask at a given lfsr threshold, what proportion of satisfying associations are incorrectly signed. **PTA:** Proportion of True Associations, **PSA:** Proportion Significant Associations.

maximum effect and thus the number of tissues greater than 50% of the maximum effect would be 1 (the effect used to normalize). We can apply this heterogeneity index, here deemed '**HI**' to the real data, but first wanted to demonstrate the superiority of MASH in estimating these quantities on simulated data. To quantity the ability of each method to accurately ascertain the heterogeneity, we can compute the heterogeneity index of the real data, and the inferred quantities, and use a modified RMSE:

$$\text{RMSE}_{\text{HI}} \sqrt{\left( \sum (\text{true}_{\text{HI}} - \text{estimated}_{\text{HI}})^2 \right)} \quad (3)$$

**Table 3.** Accuracy Comparison: RMSE

Inference Method	MASH	ASH	mash-lite
$\text{HI}_S$	39.38	40.87	39.78
$\text{HI}_{TS}$	39.98	40.77	39.51

### 1.1.1 Adaptive Shrinkage: The Multivariate Approach

To demonstrate the utility of shrinking effect-size estimates jointly, we consider the estimated effect-sizes against their observed input summary statistics using our joint (MASH) and comparing to a univariate shrinkage method (Ash). On simulated data, we can also then plot the estimated effect-sizes against the true values, again comparing among methods. Here, we show the results under the setting of tissue specificity, to analyze the behavior of eQTL of each class.

In a univariate method, all effects with the same observed effect-size  $\hat{b}_{jr}$  and standard error  $\hat{s}_{jr}$  and accordingly the same Z statistic will be shrunk equivalently, while a joint method allows us to consider effects in other tissues in augmenting the posterior estimated effect-size and its corresponding estimate of significance. In this simulated data-set, where there is an abundance of small effects, both univariate and multivariate methods tend to shrink small observed values of  $\hat{b}$  towards prior mean at  $\mathbf{0}$  as their likelihoods will be maximized by component with small  $\omega$ . However, while

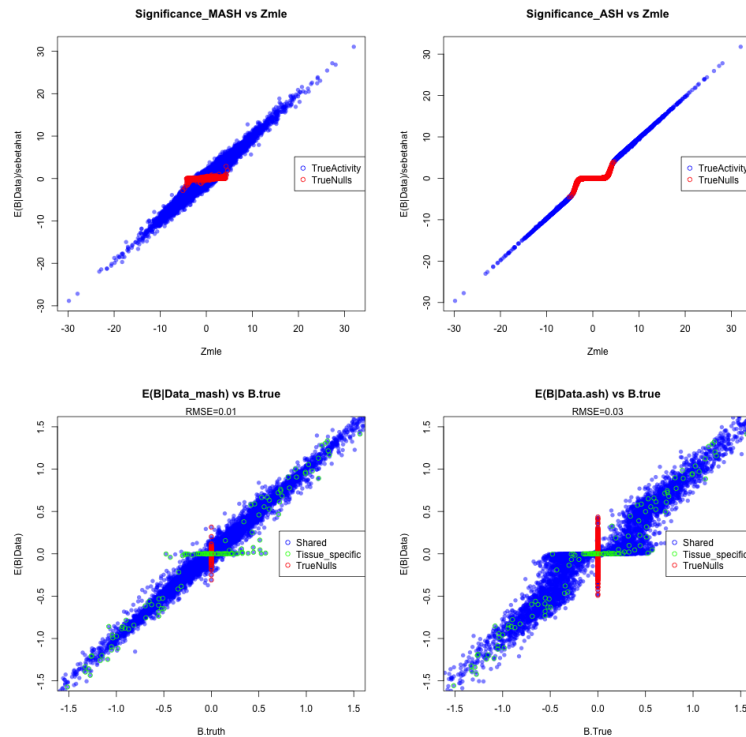


**Figure 2. Understanding Power and Accuracy Gains:** **Top:** We contrast the power advantage of a joint shrinkage approach (left) with that of a univariate thresholding approach (right), in which all observed statistics of a given level of significance shrunk equivalently, independent of the information contained in other tissues. Using the information contained in other tissues allows us to augment (or shrink less harshly) small effects in one tissue in the presence of evidence of strong effects in other tissues, while univariate methods ignore alternative tissues. Thus the method is dually ‘adaptive’ by considering the abundance of both effect-sizes (here, an abundance of small effects) and shapes in the overall data-set. **Bottom:** the correlation with the true (simulated) effect-sizes values is greater using MASH (left) than univariate methods (right), and truly null values are shrunk more harshly, while retaining the ability to capture tissue-specific eQTL.

univariate methods shrink all observed Z statistics uniformly, thus preserving their rank-order of significance, MASH does not. Critically, this is due to the power of joint analysis to consider the effects across tissues in inferring the final vector of effect-sizes, and allowing evidence contained in all tissues jointly to augment our posterior estimate of significance. Thus the method is dually ‘adaptive’ by considering the abundance of both effect-sizes and shapes in the overall data-set. Here, acknowledging consistency, small effects in one tissue will be augmented in the presence of larger effects in other tissues, resulting in dramatic power increases (Figure ??).

Furthermore, when we plot the estimated effects  $E(\beta_{jr}|Data)$  against true effect-size  $\beta_{jr}$  (Figure 2, **bottom**) and segregate these effects by class (e.g., active and shared, active and tissue-specific, or null), we see that the correlation among the true and estimated effect  $E(\beta|D)$  sizes is much tighter using our multivariate approach. Similarly, truly null effects are shrunk more tightly, due to the fact that in the presence of consistency, small effects across subgroups will lead us to have a high prior belief that an additional small observed effect in that eQTL is also likely to be close to 0. Importantly, tissue-specific QTLs are still captured using our joint approach, demonstrating that if tissue-specific patterns exist in the data, our prior belief will capture this phenomenon and accordingly our posterior estimates will reflect the underlying tissue-specific nature at a given tissue-specific SNP.

Together, these results demonstrate the tremendous power increase of using a multivariate method and the accuracy of estimating patterns of sharing from the data rather than imposing forced configurations which fail to capture the heterogeneity of effect-sizes among tissues.

### 1.1.2 Power and Adaptive Shrinkage: Real Data

Now, we consider the results of our analysis, when applied to the GTEx data set. After estimating the covariance matrices from the strongest gene-snp pairs, in an effort to capture the underlying ‘true patterns’ of sharing in the data and adding the qualitatively specific configurations ‘mash-lite’ configurations, we can infer the relative frequency of each pattern of sharing and corresponding effect-sizes from a large sample of 40,000 gene-snp pairs (see Methods for details on prior weight estimation).

Here, we report the analysis on the top SNP for each of 16,069 genes, where the ‘top’ snp is defined as the SNP with the largest observed univariate Z-statistic in absolute value across tissues. As described above and demonstrated in simulations, in the setting of an abundance of small effects in data set, MASH tends to shrink small observed values towards the prior mean at 0. It should be noted that this is a result specific to a particular data set, and in that sense ‘adaptive’ - indeed, if small effects were rare and large effects abundant, such shrinkage would not occur.

But perhaps more importantly, there is a striking increase in power (Table 5) when compared to univariate methods. There are a total of 44 tissues x 16,069 gene-snp pair associations considered, or 707,036 total tissue-level effect-size coefficients. At an  $lfsr$  threshold of 0.05, we identify 393,414 significant snp-gene-tissue effects ( $b_{jr}$ ). Using estimates shrunk according to a univariate approach (again, Ash), we identify only 91,755, meaning that using univariate methods we would be confident our ability to identify the sign in only 13% of cases, while using our joint procedure for estimating effects, we would confidently argue the SNP has a non-zero effect for a gene in a particular tissue over half (55%) of the time. As described, this tremendous increase in power arises from the fact that in the presence of a data set possessing consistency, as learned by the hierarchical model, small effects in the presence of a gene containing large effects in alternative tissues will be augmented to reflect such consistency (see Figure 3), thus increasing our confidence in its size and direction. Indeed, examining the proportion of QTL that are shared between each pair of tissues at a given significance

threshold, we see that the vast majority of tissues share greater than 60% of the significant QTL contained in both tissues (see Figure 3 at right) though there are several tissues - Whole Blood, Testes, and Transformed Cell Types - which exhibit tissue-specific behavior (see Section 1.3 for more details).

While the number of associations captured is slightly greater using the mash-lite approach, we note that the likelihood of the data set under this configuration-based model is much much worse ( $-1298672$  vs  $-1267997.5$ , see supplementary data ‘Testing and Training’ procedure) and thus represent erroneous associations. Critically, ‘mash-lite’ would put the vast majority of the prior weight on the fully ‘consistent’ configuration (Supplementary Figure 10), as SNPs demonstrating activity across all tissues, regardless of how heterogeneous among subgroups, are forced into this configuration. Simulations above demonstrate the lack of accuracy arising from such an approach.

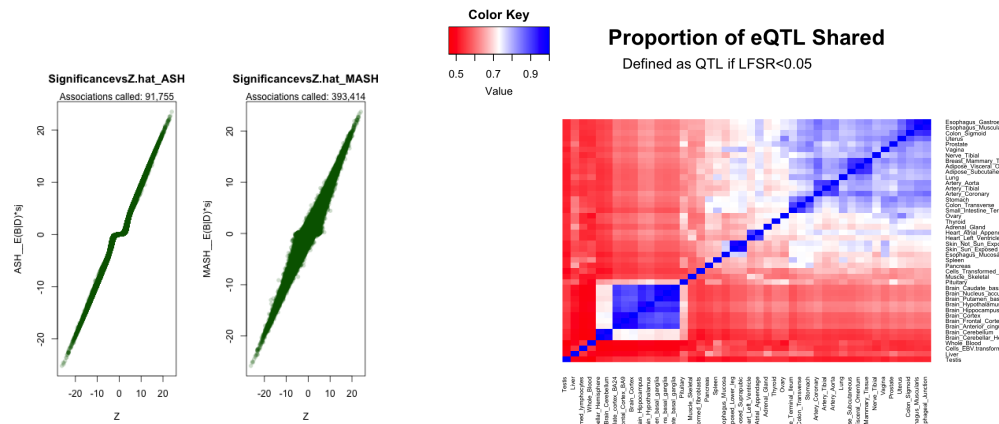


**Figure 3. Power of Joint Analysis in Real Data** From real data: Z statistics of the same size are shrunk differently depending on the effect across tissues using our joint approach MASH (**Left panel, at right**), when compared to univariate methods (**left panel, at left**), which tend to shrink all observed effects of a given size and standard error (i.e., equivalent Z statistics) uniformly, resulting in tremendous power gains (Table 5) by the increased significance induced. The increased power is due to the fact that most pairs of tissues share a majority of the QTL called by each, as defined by  $P_{shared} = \frac{QTL_i \cap QTL_j}{QTL_i \cup QTL_j}$

**Table 4. Power Comparison**

Metric	LFSR <sub>MASH</sub>	LFSR <sub>ASH</sub>	mash-lite
Significant $b_{jr} \leq 0.05$	393,414	91,755	401,552

**Table 5. Power** Restricting our analysis to thresholding by local false sign rates, we can quantify the number of associations we identify at a given local false sign rate threshold using the original summary statistics and posterior means computed using multivariate MASH and Univariate Ash. We can see that MASH calls over four times as many associations significant when compared to univariate approach, and is comparable in power to a less-accurate joint approach (mash-lite)

## 1.2 A qualitative description of heterogeneity in the GTEx data

Indeed, from the prior weight assigned to the ‘learned matrices’ (Figure 10) coupled with the simulation results in the previous sections, we can see that MASH is able to accurately parse shared configurations, thus resolving the relationship among tissues in which the QTL is active Figure 10, 4 and Supplementary Figure 9. To emphasize the contrast between our approach and existing joint methods on this data-set, we compare our results to a configuration approach which recognizes only patterns constrained to lie along the x and y axis or along the  $x - y$  line (Figure 1). MASH allows for patterns which show consistently larger effects in one tissue over another, with varying amounts of correlation among tissues. We compare the first principal component of each of these covariance matrices reflecting the patterns ‘learned’ from the data and used as  $U_k$  to model the effect-size for each gene-snp pair  $b_j$  in Equation 1 (see Methods 2.1 for details). Intuitively, this provides a single-rank ‘summary’ of the relationship in effect-sizes among tissues (Figure 4) captured by each pattern.

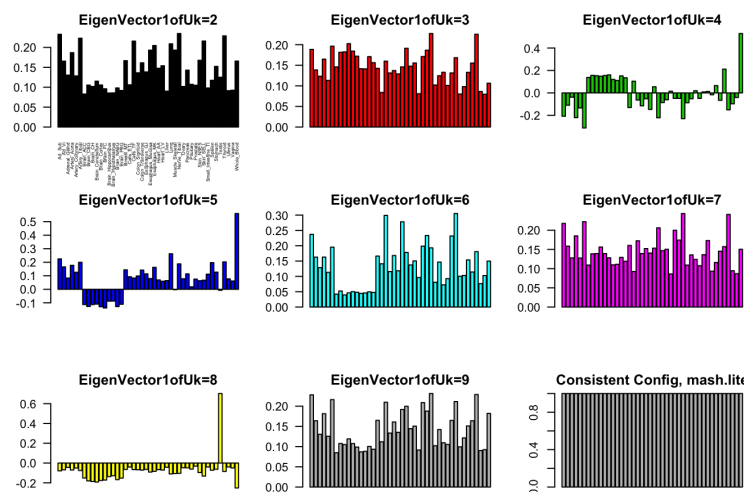


**Figure 4. Relationships Among Tissues Captured** Here, we demonstrate the first principal direction of each pattern of effects across tissues, by simply taking the first eigenvector of each of these covariance matrices. Intuitively, these provide a rank 1 summary of the relationship in effect-sizes and directions among tissues captured by each pattern. They can be contrasted with the ‘consistent configuration’ which assumes the same effect-size for all tissues in which the tissue is active. See Text for details and possible interpretations, and Supplement for guide to tissue abbreviations.

Each of the  $U_k$  thus reflects diverse relationships in effect-sizes among tissues: for instance, comparing the black and red pattern, we see that gene-snp pairs with high posterior probability of arising from the black class ( $U_k = 2$ ) demonstrate consistently smaller and shared effects in brain than other tissues, while gene-snp pairs of the red class ( $U_k = 3$ ) demonstrate strong effects in brain as compared to alternative tissues, for example. Indeed, matrix  $U_k = 3$  captures gene-snp pairs with large, correlated effects in brain, and is the most prevalent pattern of sharing in the larger data set, as reflected by its prior weight summed across effect-size (see Figure 10). Matrix  $U_k = 2$  captures SNPs with small effects in brain and larger effects in thyroid and transformed cell-types (e.g., fibroblasts, lymphocytes). Similarly, we see that the patterns learned in  $U_k = 4, 5$  and  $8$  (blue and yellow) demonstrate a degree of ‘quantitative’ specificity: that is,

consistently stronger effects in one tissue (whole blood, whole blood and testes, respectively) without restricting the effect-sizes to zero in alternative tissues. Because these patterns and their relative abundance are ‘learned’ from the data and allow for a superior model fit to methods which restrict effects as ‘active’ or ‘qualitatively specific’, we can use these to understand gross patterns present in the data as well as gene-snp specific effects. Examining the barplot (Figure 10) of the relative importance of each of these patterns as learned from the data through empirical Bayes Methods (See methods 324  
2.4) and comparing it with a method which simply calls effects ‘active or inactive’ 325  
(mash-lite) we see that such patterns are able to effectively ‘dissect’ the activity 326  
quantified in a fully ‘consistent’ configuration. 327  
328  
329  
330  
331  
332  
333

### 1.2.1 Examples of Select Patterns

Here we examine several example gene-snp pairs with a high posterior probability of arising from the covariance patterns captured by our model. We deem this posterior probability of arising from a particular pattern as a high ‘loading’ or ‘responsibility.’ We consider the posterior effect, as normalized by its standard error, to see how the significance across tissue combines information contained in the prior pattern which the gene-snp pair most resembles, and the data originally observed. 334  
335  
336  
337  
338  
339  
340  
341  
342  
343  
344  
345  
346  
347  
348  
349  
350  
351  
352

In this particular example (Figure 5, top), with high posterior probability of arising from the pattern captured by  $U_k = 3$ , strong, shared effects in brain tissues match an underlying pattern of shared effects present in the larger data set and thus allow this gene-snp pair to find its true match. Brain effect-sizes thus borrow strength from one another, and accordingly, the posterior estimates tend to nudge the brains towards a consistent, shared effect. Similarly, an overall tendency towards consistency in sign in the larger data set, as captured by the hierarchical model and reflected in the positive correlation in sign among all tissues, tends to ‘flip’ erratic off directions towards the prevailing positive direction. Heterogeneity in magnitude as captured by the model among the other tissues is reflected in the variety of banding intensity along the diagonal of the covariance matrix and in the range of heights in the barplot of eigenvector one, and reflected in the variety of non-zero effects. 353  
354  
355  
356  
357  
358  
359  
360  
361  
362  
363  
364  
365  
366  
367  
368  
369  
370  
371  
372  
373  
374

In this example (Figure 5, center), though the particular pattern featured ( $U_k = 5$ ) captures correlation in sign among all tissues, significant quantitative heterogeneity is again reflected in the dramatic range of heights in the rank 1 approximation of the direction specified by this particular covariance matrix, in this case dramatically dichotomous between whole blood and all other tissues. Here, we introduce the idea of quantitative specificity - e.g., that a SNP can be modestly ‘active’ in all tissues though to dramatically different degrees. Here, though this matrix was learned (and not forced, as in mash-lite) from the data, the pattern of quantitative tissue specificity in whole blood is evident, and we accurately reflect our suspicion about the few ‘erratic’ off directions and accordingly shrink their effects. We refer to this as quantitative specificity, because the effects are quantitatively unique to particular tissues - e.g., significantly larger in magnitude in whole blood than all other tissues - and yet considered non-zero in many tissues. This is in contrast to qualitative specificity, described below, in which we would conclude that the QTL is active in only one tissue. 353  
354  
355  
356  
357  
358  
359  
360  
361  
362  
363  
364  
365  
366  
367  
368  
369  
370  
371  
372  
373  
374

Lastly, the inclusion of the mash-lite configurations (in which the SNP has a non-zero effect in only one tissue) coupled with the learned patterns of tissue specificity evident in matrices  $U_k : 5 – 9$  serve to allow the preservation of qualitatively specific effects. Here, we show (Figure 5, bottom) a gene-snp pair demonstrating high loading on one of the mash-lite configuration matrices - indeed, we reject the significance of the effect-size estimates in all tissues but whole blood, a pattern consistent with the presence of tissue-specificity described below. Together, these results cement the resolution afforded by methods which can distinguish among tissues in which a QTL is called active, 353  
354  
355  
356  
357  
358  
359  
360  
361  
362  
363  
364  
365  
366  
367  
368  
369  
370  
371  
372  
373  
374

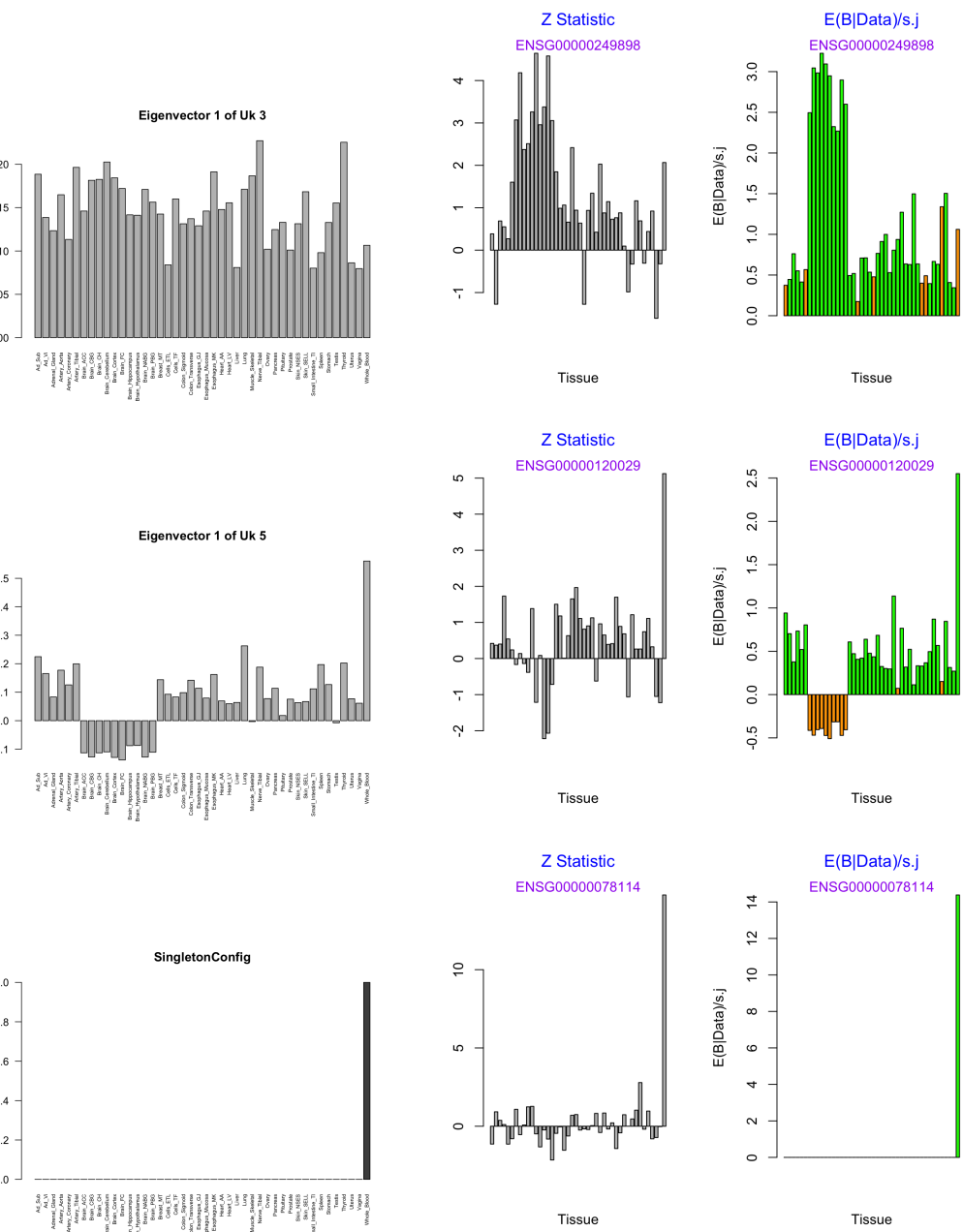


**Figure 5. High loading on  $U_k=3$ ,  $U_k=5$ , and mash-lite:** While all matrices appear to capture overwhelming correlation in sign, the varying degrees of quantitative heterogeneity in magnitude along the diagonal emphasize the utility of continuous approach. The correlation in sign means that erratic ‘off-directions’ in observed statistics are often flipped (**top**). **Center:** this gene SNP-pair demonstrates high loading on the learned (as opposed to forced) pattern of activity  $U_k = 5$  which captures quantitatively specific activity in whole blood. Effects are significant in many tissues, but quantitatively specific to whole blood. **Bottom:** we also find evidence of qualitative heterogeneity, reflected in the example demonstrating high loading on mash-lite configuration matrix, and accordingly only the activity in whole blood is deemed significant.

beyond reducing genetic effects to binary ‘on’ or ‘off’ conclusions. Importantly we have verified that this is not due to tissue-specific expression patterns (Supplement).

### 1.3 Tissue Specificity

One of the criticisms of a joint approach might be its loss of tissue-specificity. That is, by considering effects across subgroups in estimating the effect-size, one might lose sight of tissue-specific activity when it exists. Here, we demonstrate our ability to recognize such specificity both quantitatively, as described above through learned patterns of sharing which specify consistently larger effects in one tissue over others, and qualitatively through forced prior effect-size mass on  $\mathbf{0}$ . For each tissue, we can ask how many gene-snp pairs meet a given significance threshold in that tissue alone. Furthermore, tissue specific eQTL demonstrate the smoothing feature of this joint shrinkage approach: for gene-SNP pairs which demonstrate strong effects in only one tissue, the weaker erratic tissue are shrunk towards the prior mean at  $\mathbf{0}$ , resulting in a tissue specific smoothing (Figure 6, at right). We recognize an enrichment of tissue-specific effects in the transformed cell types, testes, whole blood, and thyroid.

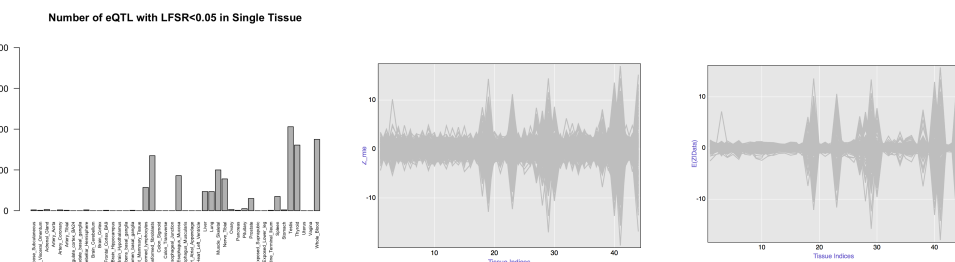


**Figure 6. Tissue Specificity** At an LFSR threshold of 0.05, we can ask how many QTL are specific to a given tissue. Several patterns of tissue-specific QTLs stand out: transformed cell types, testis, thyroid, and whole blood. Tissue specific eQTL demonstrate the smoothing feature of this joint shrinkage approach

### 1.4 Quantifying Heterogeneity

Armed with a vector of effect-size estimates across 44 tissues,  $\mathbf{b}_j$ , we can move beyond asking in how many tissues is a given gene-snp pair significant (Figure 7), and ask about the relationship in effect-size and direction among tissues in which the gene-snp pair is active.

From a biological standpoint, we might predict that effects of a different sign are rare. Considering these results with and without the inclusion of the brain tissues, which appear to behave as a strongly correlated group, we observe several phenomenon. The majority of gene-snp pairs are consistent in sign (indeed, only about 20% of genes show two significant effects of a different sign when including brain, and even fewer (14.8%) when excluding brains, see Table 6). Removing brains from our analysis tends to push the tendency towards consistency, suggesting that brain appears to behave as a large tissue-specific entity. After normalizing each gene-snp effect-size coefficient  $b_{jr}$  by the effect-size with the maximum value for the gene, we can also ask what proportion of these are positive. We again recognize homogeneity with 83% (all tissues) and 87% (excluding brain) demonstrating positive normalized effects, respectively.

Furthermore, we can now quantify the heterogeneity index in magnitude described in the simulation framework above, and ask, for each gene, in how many tissues is the

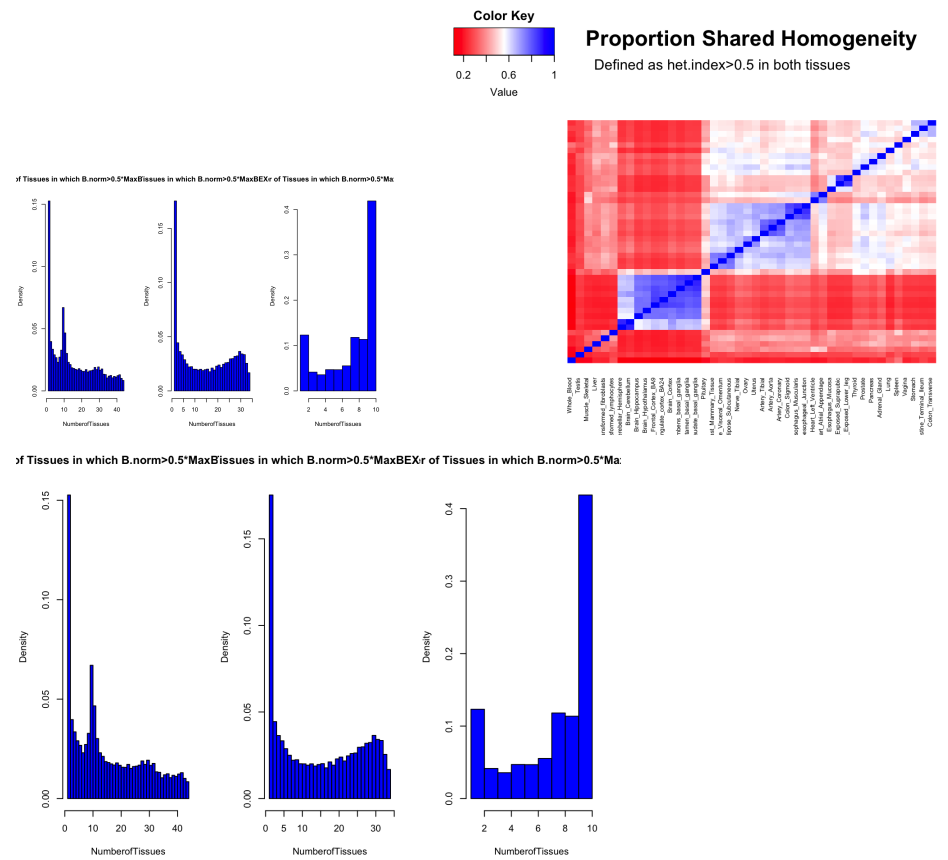


**Figure 7. Top Left:** Number of Tissues Significant At a given LFSR threshold (0.05), we can ask for each QTL, in how many tissues is it considered ‘significant’. However, armed with new information about effect-size we can ask additional questions about heterogeneity, **Bottom: Heterogeneity in Magnitude:** For each gene-snp pair, we can ask how many tissues is the effect at least 50% of the maximal effect. We consider the distribution of this ‘Heterogeneity Index’ with and without brains included in the analysis. **Upper right**, once the effects have been normalized, we ask which tissue-level are similar in magnitude to each other and to the tissue with maximum effect.

effect greater than or equal to a significant fraction, here 50% of the maximum effect (7). Genes binned in the left of this distribution are quantitatively specific because the effect is close to the maximal effect in few tissues, while homogenous genes will be featured towards the right of the distribution (maximal value at 44) as the majority of their effects across tissues are similar in magnitude. Again, excluding brain from the analysis tends to nudge us towards a belief in consistency (Table 6). To understand this sharing at the tissue level, in addition to our previous plot of pairwise sharing of significant effects (Figure 3), we can now consider the proportion of genes which have effects that are similar to one another and to the maximum effect among each pair of tissues. We recognize familiar, organ level patterns of sharing of effect-sizes, as we can see that brain-tissue effects are often similar to one another, as are vascular effects (tibial and coronary arteries), and gut tissues (esophagus and colon, as well as the terminal ilium of the small intestine and colon). This emphasizes the utility of a joint approach which can make use of subtler patterns of effect-size sharing among tissues. Taken together, these results suggest the presence of consistency in sign in our data set, and a bimodal distribution of heterogeneity in magnitude, with certain groups of tissues exhibiting sharing of effect-sizes more frequently.

**Table 6.** Heterogeneity Comparison

Data	All Tissues	No Brains
Consistent in Sign $E(b_{jrnorm} D) > 0)$	0.833	0.880
$E(\text{Consistent SignPosteriorMean}   \text{LFSR} \leq 0.05)$	0.802	0.852
$E(\text{At least 50\% max value})$	0.354	0.449

**Table 7. Heterogeneity Analysis** After normalizing each gene-snp-effect-size coefficient by the effect-size with maximal value at that gene ( $b_{jr}$ ), we can ask how many of these gene-snp effect coefficients are positive. Similarly, at a given significance threshold, we can ask how many gene-pairs contain effects of different signs across tissues. At an arbitrary LFSR threshold of 0.05 for instance, we note that 80% of genes are homogenous in sign when all tissues are considered. Excluding brains from our analysis, this rises to 85%. To evaluate consistency in magnitude, we can ask how many gene-snp-tissue effects are greater than 50% of the maximal effect across tissues for the pair. Again, we see that excluding brains from our analysis tends to push this towards consistency.

Attempting to understand which genes tend to behave the most homogeneously or heterogeneously, we can plot (Figure 8) the value used to normalize each gene, e.g., the ‘maximum’ effect-size across tissue of the gene, against the normalized values. We can see that if a large effect is present, it tends to be in the presence of homogenous effects across subgroups, while small normalizing effects tend to be in the presence of effects that are more variable in sign and magnitude. Furthermore, aggregating the gene-snp pairs at a given heterogeneity index and classifying them by the effect used to normalize (e.g., the ‘max effect’) we can see that gene-snp pairs with greater Heterogeneity Indices tend to have larger effects on average, and the tissue-specific patterns again become more evident by plotting these QTL across tissues (Figure 8, far right).

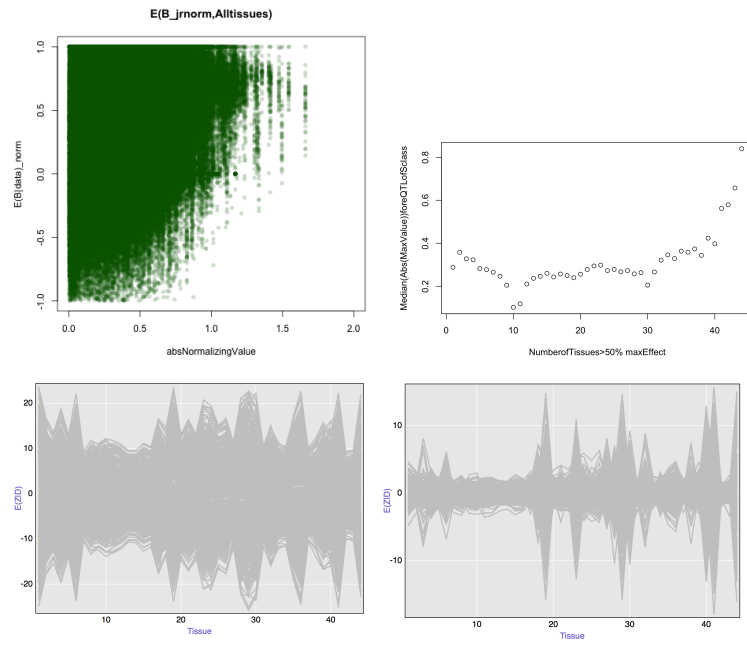


**Figure 8. Understanding Which Effects are the most Homogenous.** For each gene-snp pair, we plot the normalized gene-snp-tissue-effect (e.g.,  $b_{jr}$ ) against the largest absolute effect-size for the genes. To learn which genes are more quantitatively homogeneous, we can see that eQTLs in which a large effect is present tend to have more consistent effects across the board, and thus occur in the presence of many normalize  $b_{jr}$  close to 1. Furthermore, aggregating genes by their Heterogeneity Index and reporting the median maximal effect for genes of a given H class, we see that the maximum value tends to increase with homogeneity. We can segregate homogenous and heterogenous eQTL and consider their activity across tissues.

## 2 Discussion

In estimating the effect size of a gene-snp pair across many tissues, we have revealed new multivariate-patterns of heterogeneity and broadened our understanding of genetic effects beyond that of traditional ‘binary’ analyses. Understanding such patterns may prove invaluable in assessing the genetic impact on multi-tissue phenotypes and grouping gene-snp pairs by similar multi-tissue patterns of heterogeneity, as well as in grouping tissues which tend to respond to genetic effects similarly. Our novel approach is the first of its kind to consider the continuous heterogeneity here evident, as well as to offer an analyses of a data-set of this size (44 tissues) as previous studies [?]. While the power improvement of joint analyses has been established [3] never before has such an analyses also considered quantitative heterogeneity among effects deemed ‘shared’. Furthermore, in developing a method for such analyses, it is possible to broaden its application to any assessment of multi-subgroup effects. The Likelihood-based training algorithm we describe allows our model the flexibility of adding and removing the appropriate number of covariance matrices from the ultimate estimation.

Here, we present work on one-snp per gene, but as mentioned, armed with the hierarchical prior information from the overall data-set it is possible to infer a vector of estimated effects for any number of gene-snp pairs. Genetics is only one potential application of our approach. Our method applies broadly to any multivariate data set in which knowledge about a particular effect can be informed by its activity across subgroups. In an application of our method to the lipid data set (*Willer et al, 2013*) in which summary statistics associating genotype with LDL, HDL, Total Cholesterol and Triglycerides were assessed independently, we found our method to be more powerful than existing joint approaches and more accurate, as evaluated by likelihood of training and testing sets (see Supplement).

## Materials and Methods

Let  $\mathbf{b}_j$  represents the genetic effect of SNP-gene pair  $j$  across  $R = 44$  tissues.  
460  
We assume the following mixture prior for the  $R$  dimensional vector of true effects,  
461  
462

$$\mathbf{b}_j | \boldsymbol{\pi}, \mathbf{U}, \boldsymbol{\omega} \sim \sum_{\mathbf{k}, l} \pi_{\mathbf{k}, l} N_{\mathbf{R}}(\cdot; \mathbf{0}, \omega_l \mathbf{U}_{\mathbf{k}}) \quad (4)$$

Where  $N_{\mathbf{R}}(\cdot; \mathbf{0}, \omega_l \mathbf{U}_k)$  denotes the density of a normal distribution with mean  $\mathbf{0}$  and  
463  
variance  $\omega_l \mathbf{U}_k$ .  
464

Each component of the mixture distribution is characterized by these prior  
465  
covariance matrices,  $\mathbf{U}_k$  which capture the pattern of effects across tissues. Critically,  
466  
this prior distribution is the same for all  $J$  - hence the hierarchical incorporation of  
467  
shared information.  
468

### 2.1 Covariance Matrices

For a given  $\omega_l$ , we specify 4 ‘types’ of  $R \times R$  prior covariance matrices  $\mathbf{U}_{k,l}$ .  
469

1.  $\mathbf{U}_{k=1,l} = \omega_l \mathbf{I}_R$   
471
2.  $\mathbf{U}_{k=2,l} = \omega_l \mathbf{X}_z$  The (naively) estimated tissue covariance matrix as estimated from  
472  
the column-centered  $J \times R$  matrix of  $Z$  statistics,  $Z_{center} = \frac{1}{J} Z_{center}^t Z_{center}$   
473
3.  $\mathbf{U}_{k=3,l} = \omega_l \frac{1}{J} V_{1...p} d_{1...p}^2 V_{1...p}^t$  is the rank  $p$  eigenvector approximation of the  
474  
tissue covariance matrices, i.e., the sum of the first  $p$  eigenvector approximations,  
475  
where  $V_{1...p}$  represent the eigenvectors of the covariance matrix of tissues and  $d_{1...p}$   
476  
are the first  $p$  eigenvalues.  
477
4.  $\mathbf{U}_{k=4:4+Q-1,l} = \frac{1}{J} ((\Lambda \mathbf{F})^t \Lambda \mathbf{F})_q$  corresponding to the  $q_{th}$  sparse factor  
478  
representation of the tissue covariance matrix  
479
5.  $\mathbf{U}_{k=4+Q,l} = \frac{1}{J} (\Lambda \mathbf{F})^t \Lambda \mathbf{F}$  is the sparse factor representation of the tissue covariance  
480  
matrix, estimated using all  $q$  factors.  
481
6.  $\mathbf{U}_{k=5+Q:R+4+Q,l} = \frac{1}{J} ([100...]' [100...])$   
482
7.  $\mathbf{U}_{k=R+5+Q,l} = \frac{1}{J} ([111...]' [111...])$   
483
8. [1000...] or [111...] represent configurations such that given membership,  $\mathbf{b}_j$  arise  
484  
from the same prior variance.  
485

Critically, the computations above are estimated using the strongest snp per gene as  
486  
characterized by the maximum absolute value across  $R$  tissues, in order to optimally  
487  
initialize a ‘denoised’ matrix of the true effects.  
488

### 2.2 Deconvolution

To retrieve a ‘denoised’ or ‘deconvoluted’ estimate of the non-single rank dimensional  
490  
reduction matrices, we then perform deconvolution after initializing the EM algorithm  
491  
with the matrices specified in (2), (3) and (5). The final results of this iterative  
492  
procedure preserves the rank of the initialization matrix, and allows us to use the ‘true’  
493  
effect at each component component  $\mathbf{b}_j$  as missing data in deconvoluting the prior  
494  
covariance matrices. In brief, this algorithm works by treating not only the component  
495  
identity but also the true effect  $\mathbf{b}_j$  as unobserved data, and maximizing the likelihood  
496  
over the expectation of the complete data likelihood, considering the values  $\mathbf{b}_j$  as extra  
497  
missing data (in addition to the indicator variables  $q_{ij}$ ) (Bovy et al, 2014).  
498

Let us concatenate the list of all KxL combinations of prior covariance matrices  $U_k$  and their scaling parameters  $\omega_l$  into a KxL list and assign this length  $P$  for simplicity of notation.

Now each  $U_p$  imparts information about both *scale* and *direction*.

### 2.3 Likelihood

By maximum likelihood in each tissue separately, we can easily obtain the observed estimates of the standardized genotype effect sizes,  $\hat{\mathbf{b}}_j$ , and their observed squared standard errors recorded on the diagonal of an  $R \times R$  matrix denoted  $\hat{V}_j = (\hat{\mathbf{b}}_j)$ . We assume that the matrix of standard errors of  $\hat{\mathbf{b}}_j$ ,  $V_j$  as approximated by  $\hat{V}_j$  is diagonal and that  $\hat{V}_j$  is an accurate point estimate for the standard error and that these standard errors are independent between tissues.

If we now view  $\hat{\mathbf{b}}_j$  and  $\hat{V}_j$  as *observed data*, we can write a new “likelihood” using only the sufficient statistics,  $\hat{\mathbf{b}}_j$  and  $\hat{V}_j$ :

$$\hat{\mathbf{b}}_j | \mathbf{b}_j, \hat{V}_j \sim N_R(\hat{\mathbf{b}}_j; \mathbf{b}_j, \hat{V}_j) \quad (5)$$

In brief, though we report the analysis using  $\hat{\mathbf{b}}_j$  and its standard error, inference can be similarly performed using the vector of observed Z statistics  $Z_j$  with the matrix of squared Standard Error  $\hat{V}_j$  thus defined as the RxR Identity Matrix. This is deemed the ‘EZ’ model and assumes exchangeable standardized effects, e.g., that effects tend to scale with their standard error:

$$\frac{\mathbf{b}_j}{\hat{\mathbf{s}}_j} | \boldsymbol{\pi}, \mathbf{U}, \boldsymbol{\omega} \sim \sum_{\mathbf{k}, l} \pi_{\mathbf{k}, l} N_{\mathbf{R}}(.; \mathbf{0}, \omega_l \mathbf{U}_{\mathbf{k}}) \quad (6)$$

Likelihood based methods can then used to determine the superior model fit (see Supplement (Testing/Training) for details).

### 2.4 Mixture Weights: Estimate $\hat{\boldsymbol{\pi}}$

We wish to choose the model which best maximizes the probability of observing the data set. First, we must estimate the prior mixture weights  $\boldsymbol{\pi}$  by maximizing the likelihood

$$\begin{aligned} L(\boldsymbol{\pi}; \hat{\mathbf{b}}, \mathbf{s}) &= p(\hat{\mathbf{b}} | \mathbf{s}, \boldsymbol{\pi}) \\ &= \prod_{j=1}^J \sum_{p=1}^P \pi_p P(\hat{\mathbf{b}}_j | \hat{\mathbf{s}}_j, z_j = p) \\ &= \prod_{j=1}^J \sum_{p=1}^P \pi_p N_R(\hat{\mathbf{b}}_j; \mathbf{0}, U_p + V_j) \end{aligned} \quad (7)$$

Here, in order to obtain mixture weights  $\boldsymbol{\pi}$  which reflect the abundance of each pattern of sharing in the overall data set, we use a random set of gene-snp pairs (i.e., not restricting our analysis to the pairs with the strongest Z statistics used in the section above) and obtain the maximum likelihood estimates of the mixture weights,  $\hat{\boldsymbol{\pi}}$ , which maximize the complete data likelihood (7) (Laird 1977; Barut 2005).

- To estimate the hierarchical prior weights  $\hat{\boldsymbol{\pi}}$  we compute the likelihood at each of these randomly chosen gene-snp pairs  $j$  by evaluating the probability of observing  $\hat{\mathbf{b}}_j$  given that we know the true  $\mathbf{b}_j$  arises from component  $\mathbf{p}$  (see 5).

- Use the Expectation Maximization (EM) algorithm to estimate the optimal combination of weights as  $\hat{\pi}$  using the  $\mathbf{J} \times \mathbf{P}$  matrix of likelihoods computed according to (5).

## 2.5 Posterior Quantities

Armed with the prior mixture weights stored in the  $P$  vector  $\hat{\pi}$  we proceed to the inference step and compute the posterior weights (10) and corresponding posterior quantities across all original 16,069 gene-snp pairs.

We aim to report posterior quantities for a given gene-snp pair  $j$ . We know that for a single multivariate *Normal* the posterior on  $\mathbf{b}|U$  is simply:

$$\mathbf{b}|\hat{\mathbf{b}} \sim N_R(\tilde{\boldsymbol{\mu}}, \tilde{U})$$

where:

- $\tilde{\boldsymbol{\mu}} = \tilde{U}(\hat{V}^{-1}\hat{\mathbf{b}})$
- $\tilde{U} = (U^{-1} + \hat{V}^{-1})^{-1}$ .

Furthermore, a mixture-multivariate normal prior and a normal likelihood yields a mixture multivariate posterior, where the final posterior distribution is simply a weighted combination of multivariate normal distributions, where for each gene-snp pair  $j$  is now characterized by it's posterior mean  $\tilde{\boldsymbol{\mu}}_{jp}$  and covariance  $\tilde{U}_{jp} = (U_p^{-1} + \hat{V}_j^{-1})^{-1}$ .

$$\mathbf{b}_j|\hat{\mathbf{b}}_j, \hat{V}_j, \hat{\pi} \sim \sum_p^P \tilde{\pi}_{jp} N_R(\cdot; \tilde{\boldsymbol{\mu}}_{jp}, \tilde{U}_{jp}) \quad (9)$$

Where  $N_R(\cdot; \tilde{\boldsymbol{\mu}}_p, \tilde{U}_p)$  denotes the density of a normal distribution with mean  $\tilde{\boldsymbol{\mu}}_p$  and variance  $\tilde{U}_p$  and the posterior mixture weight  $\tilde{\pi}_p$  is simply:

$$\tilde{\pi}_{jp} = \frac{p(\hat{\mathbf{b}}_j|\hat{V}_j, z_j = p)\hat{\pi}_p}{\sum_{p=1}^P p(\hat{\mathbf{b}}_j|\hat{V}_j, z_j = p)\hat{\pi}_p} \quad (10)$$

Where  $z_j = p$  is the latent variable indicator of the component identity and each  $\hat{\pi}_p$  represents the Maximum Likelihood Estimate of the prior mixture weights assigned to each component according to (7).

## 2.6 Reported Quantities

For every gene-snp pair ‘j’, we aim to report the effect size as the posterior mean, defined as:

$$E(\mathbf{b}_j|\hat{\mathbf{b}}_j, \hat{V}_j, \hat{\pi}) = \sum_p^P \tilde{\pi}_p \tilde{\boldsymbol{\mu}}_p \quad (11)$$

And the local false sign rate, or posterior probability of incorrectly identifying the sign of the effect for a given tissues ‘r’ as :

$$P(b_{jr}) = 1 - \max[\sum_p p(b_{jr} > 0|\hat{\mathbf{b}}_j, \hat{V}_j, z_j = p)\tilde{\pi}_p, \sum_p p(b_{jr} < 0|\hat{\mathbf{b}}_j, \hat{V}_j, z_j = p)\tilde{\pi}_{jp}] \quad (12)$$

For the results section of this paper, we report the posterior mean (11) and LFSR (12) for the ‘top’ SNP per gene, but armed with the hierarchical weights computed in (7) and covariance matrices  $\mathbf{U}$  the posteriors can be computed for any gene-snp pair.

## 2.7 Simulation Framework

In brief:

1. Assemble a list of simulation covariance matrices reflecting the GTEX ‘patterns’  $\mathbf{U}$  from the 8  $U_k$  ‘learned’ from the GTEX data-set as items (2) through (5) (see Methods 2.1 for details) scaled by the maximum value along the diagonal, such that the maximal value along the diagonal of all 8  $U_k$  is 1.
2. For ‘true effects’, here 400 simulated gene-SNP pairs, choose a true-component identity  $\mathbf{z}_j = k$  by sampling with replacement from one of eight possible patterns  $U_k$
3. To simulate a variety of effects sizes along each pattern of covariance, for each of these true effect vectors  $\mathbf{b}_j$ ,  $\omega_j$  is the absolute value of the random variable  $x \sim N(\mathbf{x}; \mathbf{0}, \mathbf{1})$ .
4.  $\mathbf{b}_j | \mathbf{U}, \boldsymbol{\omega}, \mathbf{z} \sim N_{44}(.; \mathbf{0}, \omega_j \mathbf{U}_k)$ . Here,  $N_R(.; \mathbf{0}, \omega_j U_k)$  denotes the density of a normal distribution with mean  $\mathbf{0}$  and variance  $\omega_j U_k$ .
5. For all 50,000 gene SNP pairs, treat  $\mathbf{s}_j$  as known R-vector of standard error, we simulate the R vector of *Error* as  $\mathbf{E}_j \sim N(.; \mathbf{0}, V_j)$  where  $V_j$  represents the diagonalized matrix of squared known standard error,  $\mathbf{s}_j^2$ .
6. For all 50,000 gene SNP pairs,  $\hat{\mathbf{b}}_j | \mathbf{b}_j, V_j = \mathbf{b}_j + \mathbf{E}_j$  and the observed Z statistic for each gene-SNP-tissue coordinate can be obtained from this vector of estimated  $\hat{\mathbf{b}}_j$  and (known) standard error,  $\mathbf{s}_j$  as  $\frac{\hat{\mathbf{b}}_j}{\mathbf{s}_j}$ .
7. In the tissue-specific scenario, for 35% of the ‘true’ gene SNP pairs, simulate  $\mathbf{b}_j$  according to one of ‘5’ tissue-specific configurations, using the effect sizes obtained from the simulated  $\omega_j$  above, according to the sparse matrix described in item (6) (Methods 2.1).
8. Following the framework (detailed Method 2.5) perform inference on the observed summary statistics  $\hat{\mathbf{b}}_j$  to estimate the *posterior mean* (11) and *lfsr* (12) for all 50,000 gene-SNP pairs.

## Supporting Information

### 2.8 Testing and Training

In order to determine the optimal number and rank of the covariance matrices, we divide our data set into a training and test data set, each containing 8000 genes.

In the training set, we proceed as above: choosing the top SNP for each of the 8000 genes, creating a list of covariance matrices through deconvolution and grid selection of these top 'training gene-snp' pairs.

Then, within the training data, we similarly choose a random set of gene-snp pairs (restricting our analysis to genes contained in the training set). Specifically, we choose 20,000 random-gene snp pairs and use the EM algorithm to learn the mixture proportions  $\hat{\pi}$  from this data set as in (7).

We then use the KxL vector of  $\pi$  from the training set to estimate the log likelihood of each data point in the test data set. If our model is biased (or 'overfit') to the training data set, then a larger number of covariance matrices may actually decrease the test log-likelihood.

### 2.9 Visualizing All Patterns of Sharing

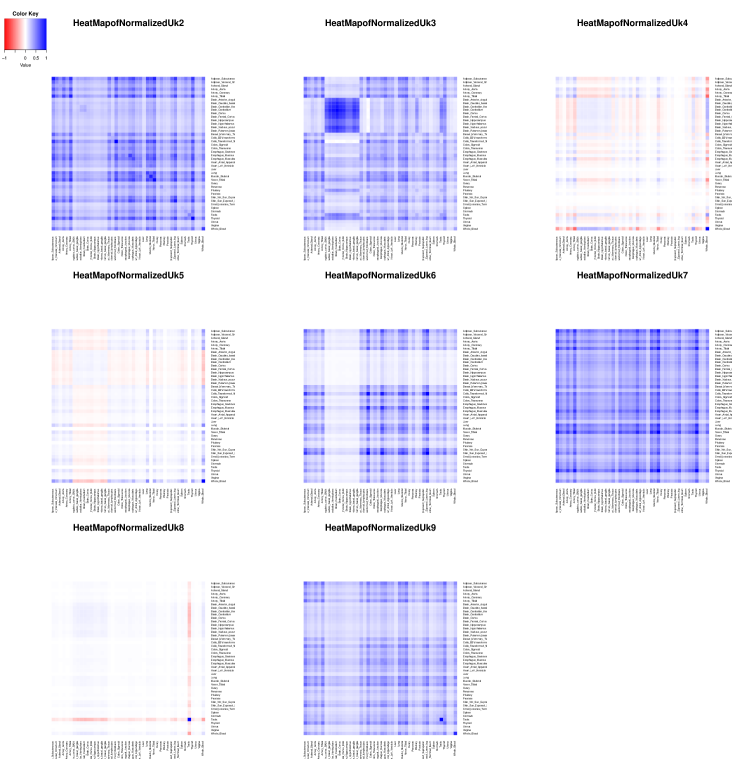


**Figure 9. Diverse Array of Relationships among tissues.** Here, we use heatmaps to visualize all the patterns of sharing present in the data

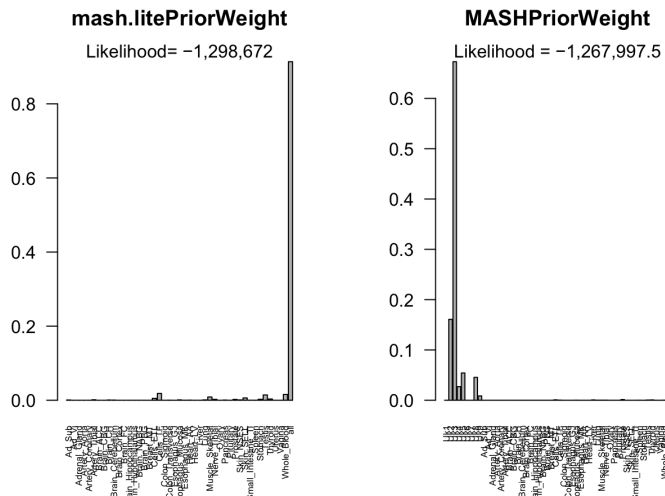


**Figure 10. Prior Weight Assigned to Patterns of Activity** While a joint method like ‘mash-lite’ assigns the majority of the prior weight to the ‘consistent’ (active across all tissues with the same prior effect-size) configuration, we can see that MASH is able to accurately parse shared configurations, thus resolving the relationship among tissues in which the QTL is active. This is a superior model fit, as judged by the likelihood improvement and simulation results above.

## Acknowledgments

## References

1. Nicolae DL, Gamazon E, Zhang W, Duan S, Dolan ME, Cox NJ. Trait-Associated SNPs Are More Likely to Be eQTLs: Annotation to Enhance Discovery from GWAS. *PLoS Genetics*. 2010 Apr;6(4). Available from: <http://www.ncbi.nlm.nih.gov/pmc/articles/PMC2848547/>.
2. Veyrieras JB, Kudaravalli S, Kim SY, Dermitzakis ET, Gilad Y, Stephens M, et al. High-Resolution Mapping of Expression-QTLs Yields Insight into Human Gene Regulation. *PLoS Genet*. 2008 Oct;4(10):e1000214. Available from: <http://dx.doi.org/10.1371/journal.pgen.1000214>.
3. Flutre T, Wen X, Pritchard J, Stephens M. A Statistical Framework for Joint eQTL Analysis in Multiple Tissues. *PLoS Genet*. 2013 May;9(5):e1003486. Available from: <http://dx.doi.org/10.1371/journal.pgen.1003486>.
4. Wen X, Stephens M. Bayesian methods for genetic association analysis with heterogeneous subgroups: From meta-analyses to gene-environment interactions. *The Annals of Applied Statistics*. 2014 Mar;8(1):176–203. ArXiv:1111.1210 [stat]. Available from: <http://arxiv.org/abs/1111.1210>.
5. Dimas AS, Deutsch S, Stranger BE, Montgomery SB, Borel C, Attar-Cohen H, et al. Common regulatory variation impacts gene expression in a cell type-dependent manner. *Science (New York, NY)*. 2009 Sep;325(5945):1246–1250.